Characterization and Optimization of Pathlength Difference in Si Waveguides on SiO for Passive Photonic Devices

Garrett Coleman (EDX name: gjcoleman) IPG Photonics

***Abstract*—This paper investigates the pathlength difference in silicon (Si) waveguides on silicon dioxide (SiO) substrates for passive photonic devices, with a focus on mode confinement, free spectral range (FSR), and interferometric performance. Simulated waveguide mode profiles were obtained using Lumerical MODE Solutions, considering a waveguide geometry with a width of 500 nm and height of 220 nm, operating under transverse electric (TE) polarization. The effective and group indices of the waveguide were extracted as a function of wavelength, and a compact model for the waveguide's behavior was developed through polynomial expressions.**

Additionally, the transfer function of the interferometer was derived as a mathematical expression to describe its wavelength-dependent performance. A parameter variation study was conducted, including different pathlength differences (L) and waveguide widths, and the corresponding FSR was calculated. Transmission spectra of photonic circuits were also simulated using Lumerical INTERCONNECT to validate the theoretical predictions. The group index was derived from the FSR of an unbalanced interferometer, and the resulting equation was tested with simulation data. Methods for extracting this information from experimental data are also discussed. These results provide insights into the design and performance optimization of Si-based passive photonic circuits.

I. Introduction

Silicon photonics has emerged as a promising technology for high-performance optical interconnects and integrated photonic circuits, owing to its compatibility with complementary metal-oxide-semiconductor (CMOS) processing and the ability to integrate with existing silicon-based electronic systems. A critical aspect of silicon photonic devices is the design and optimization of waveguides, which form the backbone of most photonic circuits. The geometry and material properties of these waveguides strongly influence their performance, especially in terms of mode confinement, propagation losses, and device characteristics such as the free spectral range (FSR) and pathlength differences (ΔL) in interferometric structures.

In particular, silicon-on-insulator (SOI) waveguides, which consist of a silicon core on a silicon dioxide (SiO_2) substrate, offer significant advantages due to their high refractive index contrast and compatibility with nanofabrication techniques. These waveguides can be engineered to support various polarization modes, with transverse electric (TE) polarization being commonly studied for its lower propagation loss and ease of integration with existing photonic devices [[1]]. The confinement of light within the core of these waveguides is essential for minimizing loss and ensuring efficient coupling between components. In addition, the pathlength difference between arms of interferometric devices, such as Mach-Zehnder interferometers (MZIs), plays a crucial role in determining the performance of optical switches and filters.

Recent advances in fabrication techniques, such as electron beam lithography, have enabled the creation of high-confinement silicon waveguides with precise control over their dimensions and structural properties [[3]]. Additionally, novel coupling methods, such as sub-wavelength grating couplers, have facilitated efficient light coupling into and out of these waveguides, which is essential for scalable photonic circuits [[4]]. However, understanding the detailed interplay between waveguide geometry, polarization, and the resulting mode profiles is crucial for optimizing device performance.

This study investigates the pathlength difference in Si waveguides on SiO_2, with a particular focus on mode confinement within the core, the effect of waveguide geometry on the free spectral range, and the performance of passive photonic devices. We explore the simulation of waveguide mode profiles using Lumerical MODE Solutions and MATLAB, and derive key equations to characterize the group index in terms of the FSR in unbalanced interferometers. The results of this work are expected to provide valuable insights for the design of Si-based passive photonic circuits.

II. Theory

The behavior of light in silicon-on-insulator (SOI) waveguides, as well as the transfer functions of passive devices like Mach-Zehnder interferometers (MZI), is governed by several key theoretical principles. In this section, we outline the key theories that underpin the analysis of waveguide geometry, mode propagation, and interferometric performance.

A. Waveguide Compact Model

In the design of silicon photonic circuits, the geometry of the waveguide significantly affects the light propagation characteristics. A waveguide can be described as a dielectric structure that confines light within a core region due to the difference in refractive indices between the core and the surrounding cladding. The compact model for waveguides is typically expressed in terms of the effective index of the waveguide, which is influenced by factors such as waveguide dimensions, the refractive index contrast, and the wavelength of operation.

For a rectangular silicon waveguide with a silicon core and silicon dioxide (SiO_2) cladding, the effective index n_{eff} can be approximated using a modal solver (e.g., from Lumerical MODE Solutions). This effective index governs the propagation constant and determines the mode confinement within the core. The waveguide mode is predominantly determined by the dimensions of the core, specifically the width w and height h,

which can be used to calculate the confinement factor and modal propagation characteristics.

The group index n_{g} is another important quantity that characterizes the velocity of light within the waveguide. The group index depends on the wavelength of operation and the refractive index of the material and is often approximated as:

$$n_{\mathrm{g}}(\lambda) = n_{\mathrm{eff}}(\lambda) + \lambda \frac{dn_{\mathrm{eff}}}{d\lambda}$$

where $n_{\mathrm{eff}}(\lambda)$ is the wavelength-dependent effective refractive index. The compact model for the effective index can be calculated using the following equation:

$$\mathrm{nef}(\lambda) = 2.44 - 1.13(\lambda - \lambda_0) - 0.03(\lambda - \lambda_0)^2$$

B. Mach-Zehnder Interferometer Transfer Function

A Mach-Zehnder interferometer (MZI) is one of the most commonly used passive devices in silicon photonics, often used for optical switching and modulation. The interferometer consists of two arms with a pathlength difference ΔL that causes a phase difference between the two arms. When light is injected into the MZI, the interference of the light in the two arms results in constructive or destructive interference depending on the phase difference.

The transfer function $T(\lambda)$ of an MZI can be derived from the interference condition. For simplicity, assume that the light is split equally between the two arms of the interferometer, and each arm introduces a phase shift $\Delta\phi = \frac{2\pi\Delta L}{\lambda}$, where ΔL is the pathlength difference and λ is the wavelength of light. The transfer function of the MZI is given by:

$$T(\lambda) = \frac{1}{2}\left(1 + \cos\left(\frac{2\pi\Delta L}{\lambda}\right)\right)$$

This equation describes how the transmission through the MZI varies with wavelength. The free spectral range (FSR) of the MZI, which is the wavelength interval over which the interference pattern repeats, can be obtained by determining the wavelength difference at which the phase difference $\Delta\phi$ changes by 2π. The FSR is given by:

$$\mathrm{FSR} = \frac{\lambda^2}{n_{\mathrm{g}}\Delta L}$$

where n_{g} is the group index of the waveguide, and ΔL is the pathlength difference between the two arms of the MZI.

C. Pathlength Difference and Interferometer Performance

The pathlength difference ΔL in the arms of the MZI directly affects the phase shift between the two arms, and thus the interference pattern. A small change in ΔL can lead to significant changes in the output signal, especially in high-sensitivity applications such as optical switching and sensing. The precise control of ΔL is critical for the accurate operation of MZIs.

In passive silicon photonic circuits, the pathlength difference is typically engineered by carefully designing the waveguide layout to ensure that both arms of the interferometer are as symmetrical as possible, with any differences compensated for by adjusting waveguide lengths. However, manufacturing variations and material properties, such as thermal expansion, can introduce variations in ΔL, which may degrade the performance of the MZI. To compensate for this, various thermal tuning techniques can be employed, such as resistive heating of the waveguide to dynamically adjust the refractive index and control the phase shift.

D. Group Index and Free Spectral Range (FSR) Estimation

The group index n_{g} plays an essential role in determining the FSR of the interferometer. By analyzing the MZI's transfer function and measuring the wavelength spacing between successive interference peaks, it is possible to extract the group index of the waveguide. This relationship is given by:

$$n_{\mathrm{g}} = \frac{\lambda^2}{\mathrm{FSR}\Delta L}$$

This equation allows for the extraction of n_{g} from experimental data and can also be tested against simulation results to verify the theoretical predictions.

In this work, simulations using Lumerical MODE Solutions and MATLAB will be used to calculate the group index as a function of wavelength, and the expected FSR will be compared against experimental data to validate the theoretical models.

III. Modeling and Simulation

A. Waveguide Properties

In this section, we will discuss the modeled waveguide properties. The passive waveguide structures modeled consist of a Silicon (Si) core of approximately 500 nm in width and 220nm in height. The waveguide is surrounded by SiO2. It was found that the effective index of the TE and TM mode were approximately 2.44 and 1.78, respectively. Also, the group index was found to be 4.2 and 3.72, respectively.

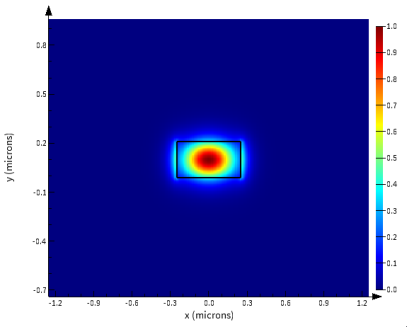

Figure 1. Modeled TE mode in Si-SiO2 passive waveguides.

Next the effective index and group index vs wavelength were explored over 1.5-1.6um range.

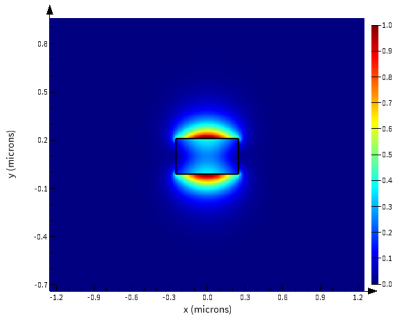

Figure 2. Modeled TM mode in Si-SiO2 passive waveguides.

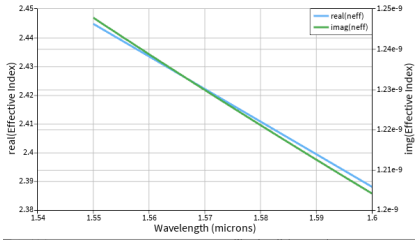

Figure 3. Effective index vs wavelength for TE mode in Si-SiO2 passive waveguide.

B. Mach-Zehnder Interferometer Modeling

In this section, we present the results from the simulations and modeling of the Mach-Zehnder interferometer (MZI) devices, focusing on key performance metrics such as the free spectral range (FSR), gain, and transmission. The following figures illustrate the performance of the MZI devices with varying path lengths. The modeled Mach-Zehnder interferometer modeled had a pitch length of 127um and other parameters noted below.

Table 1 shows the theoretical parameters for each MZI, using the compact theoretical model utilizing the path length difference (dL), transmission values (T_1 and T_2), and the calculated FSR:

The free spectral range (FSR) is calculated using the equation based on the wavelength $\lambda = 1.55\,\mu m$ and the effective index $n_{\text{eff}} = 2.44$. The path length differences (dL) for each device are provided, and the theoretical FSR is calculated for each MZI.

C. Free Spectral Range (FSR) Analysis

D. Transmission and Gain Characteristics

E. Group Velocity and Group Index Analysis

IV. Fabrication

Two chips were fabricated in this course. Either report on one dataset, or on both. Choose the text as appropriate.

A. Washington Nanofabrication Facility (WNF) silicon photonics process:

The devices were fabricated using 100 keV Electron Beam Lithography [[2]]. The fabrication used silicon-on-insulator

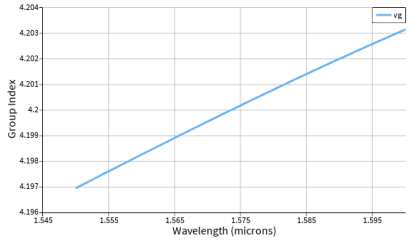

Figure 4. Group index vs wavelength for TE mode in Si-SiO2 passive waveguide.

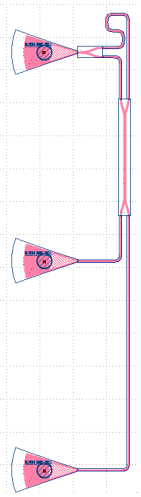

Figure 5. The design of the modeled Mach-Zehnder Interferometer.

wafer with 220 nm thick silicon on 3 μm thick silicon dioxide. The substrates were 25 mm squares diced from 150 mm wafers. After a solvent rinse and hot-plate dehydration bake, hydrogen silsesquioxane resist (HSQ, Dow-Corning XP-1541-006) was spin-coated at 4000 rpm, then hotplate baked at 80 °C for 4 minutes. Electron beam lithography was performed using a JEOL JBX-6300FS system operated at 100 keV energy, 8 nA beam current, and 500 μm exposure field size. The machine grid used for shape placement was 1 nm, while the beam stepping grid, the spacing between dwell points during the shape writing, was 6 nm. An exposure dose of 2800 μC/cm2 was used. The resist was developed by immersion in 25% tetramethylammonium hydroxide for 4 minutes, followed by a flowing deionized water rinse for 60 s, an isopropanol rinse for 10 s, and then blown dry with nitrogen. The silicon was removed from unexposed areas using inductively coupled plasma etching in an Oxford Plasmalab System 100, with a chlorine gas flow of 20 sccm, pressure of 12 mT, ICP power of 800 W, bias power of 40 W, and a platen temperature of 20 °C, resulting in a bias voltage of 185 V. During etching, chips were mounted on a 100 mm silicon carrier wafer using perfluoropolyether vacuum oil.

B. Applied Nanotools, Inc. NanoSOI process:

The photonic devices were fabricated using the NanoSOI MPW fabrication process by Applied Nanotools Inc.

Symb	L1 (um)	L2 (um)	dL (um)	CM T1 (%)	CM T2 (%)	CM FSR (nm)	FM T1 (%)	FM T2 (%)	FM FSR (nm)
MZI1	35.128	99.996	64.87	3.4%	96.6%	8.845	3.26%	91.98%	8.71
MZI2	35.128	100.036	64.91	0.0%	100.0%	8.839	0.01%	95.23%	8.723
MZI3	35.128	100.076	64.95	4.1%	95.9%	8.833	3.87%	91.36%	8.72
MZI4	35.128	100.116	64.99	15.0%	85.0%	8.827	14.28%	80.95%	8.707
MZI5	35.128	100.156	65.03	31.2%	68.8%	8.821	29.68%	65.56%	8.7064
MZI6	35.128	100.196	65.07	50.1%	49.9%	8.815	47.75%	47.48%	8.702

Table I

THEORETICAL PARAMETERS FOR THE MZI DEVICES AND THEIR CORRESPONDING FSR VALUES. CM INDICATES COMPACT MODEL AND FM INDICATES THE LUMERICAL MODELED PARAMETERS. PLEASE NOTE THAT THE TRANSMISION VALUES ARE DEFINED AT 1550NM.

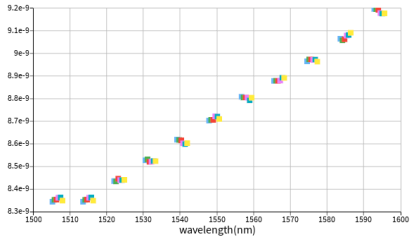

Figure 6. Free spectral range (FSR) versus path length difference for the MZI devices.

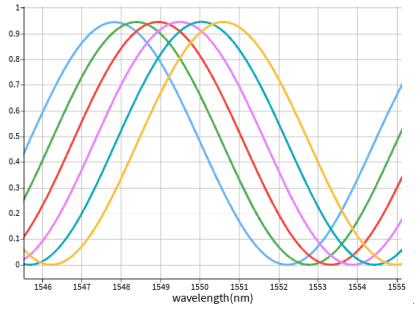

Figure 7. Zoomed-in transmission characteristics for MZI devices showing the interference pattern (set 1).

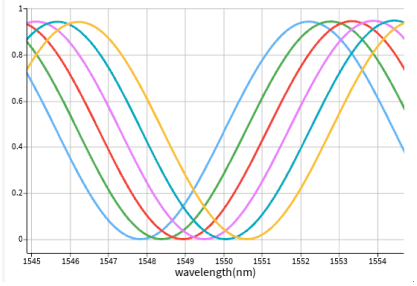

Figure 8. Zoomed-in transmission characteristics for MZI devices (set 2).

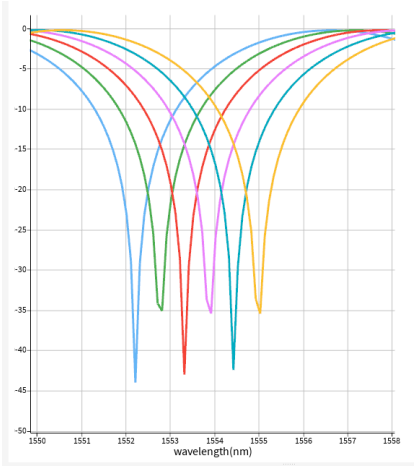

Figure 9. Gain versus path length difference for MZI devices (set 1).

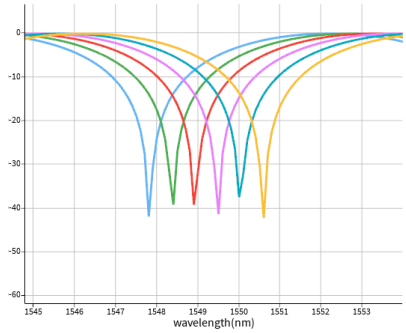

Figure 10. Gain versus path length difference for MZI devices (set 2).

(http://www.appliednt.com/nanosoi; Edmonton, Canada) which is based on direct-write 100 keV electron beam lithography technology. Silicon-on-insulator wafers of 200 mm diameter, 220 nm device thickness and 2 μm buffer oxide thickness are used as the base material for the fabrication. The wafer was pre-diced into square substrates with dimensions of 25x25 mm, and lines were scribed into the substrate backsides to facilitate easy separation into smaller chips once fabrication was complete. After an initial wafer clean using piranha solution (3:1 H2SO4:H2O2) for 15 minutes and water/IPA rinse, hydrogen silsesquioxane (HSQ) resist was spin-coated onto the substrate and heated to evaporate the solvent. The photonic devices were patterned using a Raith EBPG 5000+ electron beam instrument using a raster step size of 5 nm. The exposure dosage of the design was corrected for proximity effects that result from the backscatter of electrons from exposure of nearby features. Shape writing order was optimized for efficient patterning and minimal beam drift. After the e-beam exposure and subsequent development with a tetramethylammonium sulfate (TMAH) solution, the devices were inspected optically for residues and/or defects. The chips were then mounted on a 4" handle wafer and underwent an anisotropic ICP-RIE etch process using chlorine after qualification of the etch rate. The resist was removed from the surface of the devices using a 10:1 buffer oxide wet etch, and the devices were inspected using a scanning electron microscope (SEM) to verify patterning and etch quality. A 2.2 μm oxide cladding was deposited using a plasma-enhanced chemical vapour deposition (PECVD)

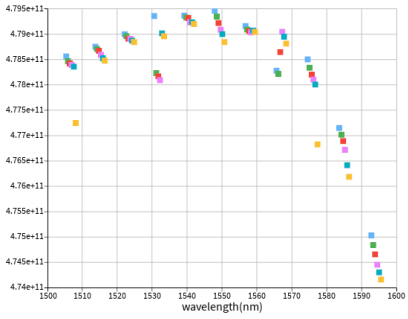

Figure 11. Group velocity versus wavelength for MZI devices with different path length differences.

process based on tetraethyl orthosilicate (TEOS) at 300ºC. Reflectrometry measurements were performed throughout the process to verify the device layer, buffer oxide and cladding thicknesses before delivery.

V. Experimental Data

To characterize the devices, a custom-built automated test setup [[3]] with automated control software written in Python was used (http://siepic.ubc.ca/probestation). An Agilent 81600B tunable laser was used as the input source and Agilent 81635A optical power sensors as the output detectors. The wavelength was swept from 1500 to 1600 nm in 10 pm steps. A polarization maintaining (PM) fibre was used to maintain the polarization state of the light, to couple the TE polarization into the grating couplers [[4]]. A 90º rotation was used to inject light into the TM grating couplers [4]. A polarization maintaining fibre array was used to couple light in/out of the chip [www.plcconnections.com].

VI. Analysis

Mach-Zehnder interferometers (MZIs) were then modeled with a pitch of 127 µm. A compact theoretical model was utilized to predict key performance metrics, including free spectral range (FSR), transmission, and gain. Using this model, path length differences, theoretical transmission percentages, and FSRs were calculated for each device. Theoretical FSR values were computed assuming a central wavelength of 1.55 µm and an effective index of 2.44. These results were compared with full simulation results obtained using Lumerical INTERCONNECT, showing strong agreement between theory and simulation.

The analysis confirmed that the FSR decreases with increasing path length difference between the arms of the MZI, consistent with theoretical expectations. Infact, it matches the compact model more closely than the data derived from LUMERICAL. This inverse relationship between FSR and path length difference was clearly observed in the simulation data. Transmission spectra were also extracted for each device, and detailed views of these spectra revealed clear periodic interference fringes, corresponding to the different L values.

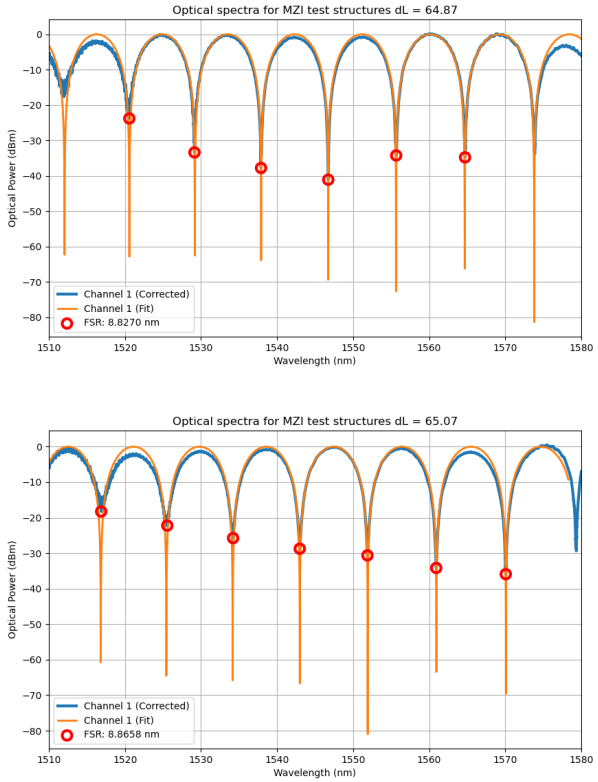

Abbildung 12. Experimental Data with curve fitted model and Free spectral range based on minima data found.

Trends in transmission and gain were evaluated, highlighting the optical performance variations across the devices.

Finally, a simulated transmission curve was fit to the experimental Mach-Zehnder interferometer (MZI) data using a least-squares fitting method implemented in a Python script. This allowed for accurate extraction of the free spectral range (FSR) and the corresponding group index. The model used for the MZI transmission was given by

$$T(\lambda) = 10\log_{10}\left(0.25 \times \left|1 + \exp\left(-i\left(\frac{2\pi\, n_{\text{eff}}(\lambda)}{\lambda} - \frac{\alpha}{2}\right)\Delta L\right)\right|^2\right),$$

where $n_{\text{eff}}(\lambda)$ is the effective index as a function of wavelength, α is the propagation loss coefficient, and ΔL is the path length difference between the MZI arms. By fitting this model to the measured data and analyzing the extracted FSR values along with the known path length differences, the group index of the waveguides was determined and compared against values obtained directly from mode simulations. The extracted group indices showed excellent agreement with the simulated results, validating both the compact modeling approach and the simulation methodologies employed throughout the study.

VII. Conclusion

The modeling and simulation of silicon photonic waveguides and Mach-Zehnder interferometers presented in this work show excellent agreement with theoretical predictions, thereby

Symb	dL (um)	Sim FSR (nm)	Sim ng	Exp FSR (nm)	% diff	Exp ng
MZI1	64.87	8.845	4.252	8.840	1.50%	4.189
MZI2	64.91	8.839	4.243	8.837	1.31%	4.188
MZI3	64.95	8.833	4.242	Nan	Nan	Nan
MZI4	64.99	8.827	4.245	8.828	1.39%	4.187
MZI5	65.03	8.821	4.243	8.816	1.26%	4.190
MZI6	65.07	8.815	4.243	8.805	1.19%	4.193

Tabelle II
COMPARISON BETWEEN THE MODELED AND EXPERIMENTAL DATA FOR THE MEASURED MZI.

validating the employed analytical and numerical methodologies. Accurate extraction of effective indices, group indices, and optical mode profiles enabled a rigorous evaluation of device performance. The compact modeling approach reliably predicted critical characteristics such as free spectral range and transmission spectra, with simulated trends, including the inverse scaling of FSR with differential path length, aligning closely with theoretical expectations. Moreover, the strong correlation between extracted and simulated group indices underscores the precision of the modeling framework. These results establish a comprehensive and reliable methodology for the predictive design, simulation, and optimization of integrated photonic circuits, significantly advancing the efficiency and fidelity of photonic device development.

VIII. ACKNOWLEDGEMENTS

I/We acknowledge the edX UBCx Phot1x Silicon Photonics Design, Fabrication and Data Analysis course, which is supported by the Natural Sciences and Engineering Research Council of Canada (NSERC) Silicon Electronic-Photonic Integrated Circuits (SiEPIC) Program. The devices were fabricated by Richard Bojko at the University of Washington Washington Nanofabrication Facility, part of the National Science Foundation's National Nanotechnology Infrastructure Network (NNIN), and Cameron Horvath at Applied Nanotools, Inc. Enxiao Luan performed the measurements at The University of British Columbia. We acknowledge Lumerical Solutions, Inc., Mathworks, Mentor Graphics, Python, and KLayout for the design software.

REFERENCES

1. Chrostowski L, Hochberg M (2015) Silicon Photonics Design. Cambridge University Press (CUP)

2. Bojko RJ, Li J, He L, et al. (2011) Electron beam lithography writing strategies for low loss high confinement silicon optical waveguides. Journal of Vacuum Science & Technology B: Microelectronics and Nanometer Structures 29:06F309. https://doi.org/10.1116/1.3653266

3. Chrostowski L, Hochberg M Testing and packaging. In: Silicon Photonics Design. Cambridge University Press (CUP), pp 381–405

4. Wang Y, Wang X, Flueckiger J, et al. (2014) Focusing sub-wavelength grating couplers with low back reflections for rapid prototyping of silicon photonic circuits. Opt Express 22:20652. https://doi.org/10.1364/oe.22.020652